Appendices and Additional Resources for "Inter-Signal Correction Sensitivity Analysis Aperture-Dependent Delays Induced by Antenna Anisotropy in Modernized GPS Dual-Frequency Navigation"

May/June 2016 issue of *Inside GNSS*

Appendix A: Relating Local Level Elevation and Azimuth to SV Nadir/Boresight Angle θ and SV azimuth

Figure A1 summarizes the geometry relationships between elevation angle E at the user antenna and angle θ at the SV transmit side. When the elevation angle E is 90 degree, the satellite is directly overhead, the nadir/boresight angle θ is 0. The satellite being directly over-head is equivalent to the user being directly below the satellite's antenna. When the elevation angle is at 5 degrees, the line of sight nadir angle at the satellite is at 13.9 degrees, which the ICD calls the Edge-of-Earth (EOE) angle. The law of sines can be used to derive an equation to relate elevation angle E to SV boresight angle θ as given in the figure A1 below.

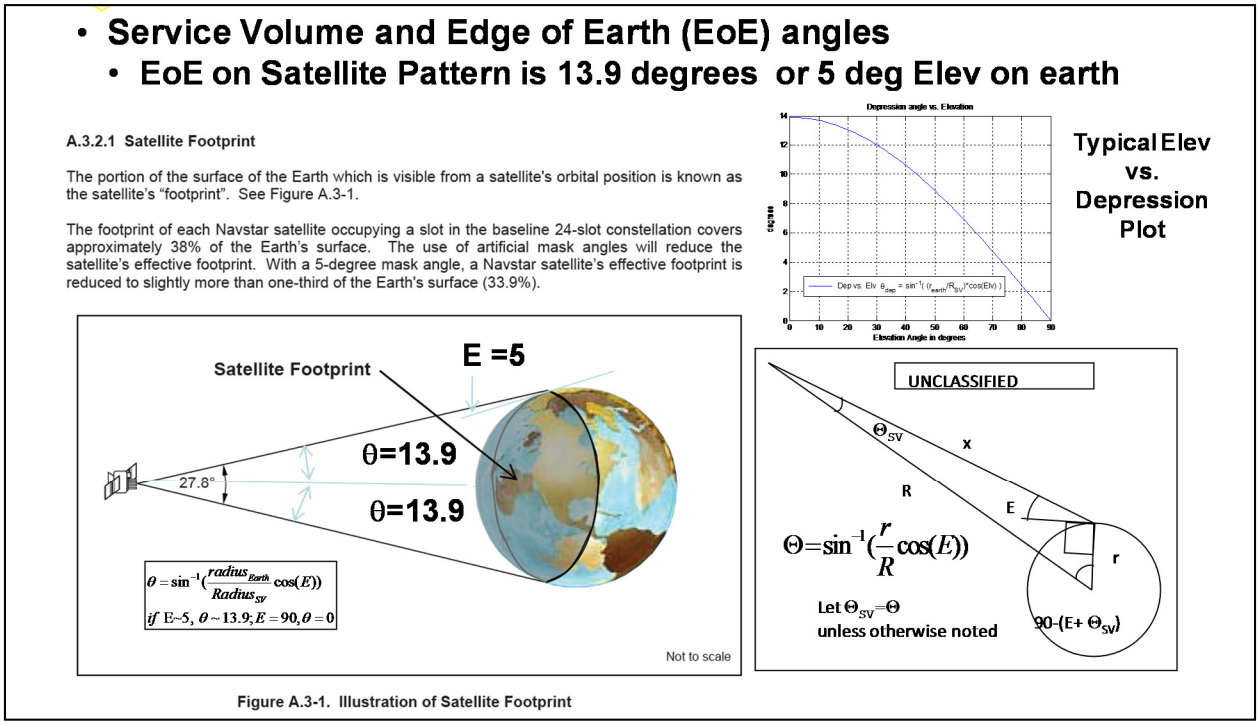

FIGURE A1: RELATIONSHIP BETWEEN ELEVATION ANGLE E AND SV NADIR /BORESIGHT ANGLE θ

As the satellite rises and sets from low to high and back down to low elevation angles, the nadir angle starts high, gets as close to 0 as the satellite approaches being overhead, and then returns back to the edge of beam at low elevation angles. Because the satellite is undergoing solar panel sun pointing, the SV is rotating and thus there is also an SV azimuth profile. If you implement the SV yaw algorithm (ref 6.2), you can take any local angle elevation and azimuth at the user location and create an equivalent SV nadir angle/SV attitude plot to map the actual path through the SV antenna. This is done in figure A2.

At a fixed location on the ground, one can only build up the full mapping of each SV antenna pattern over time. An example of how long it takes to get coverage of one SV is shown in Figure A2.

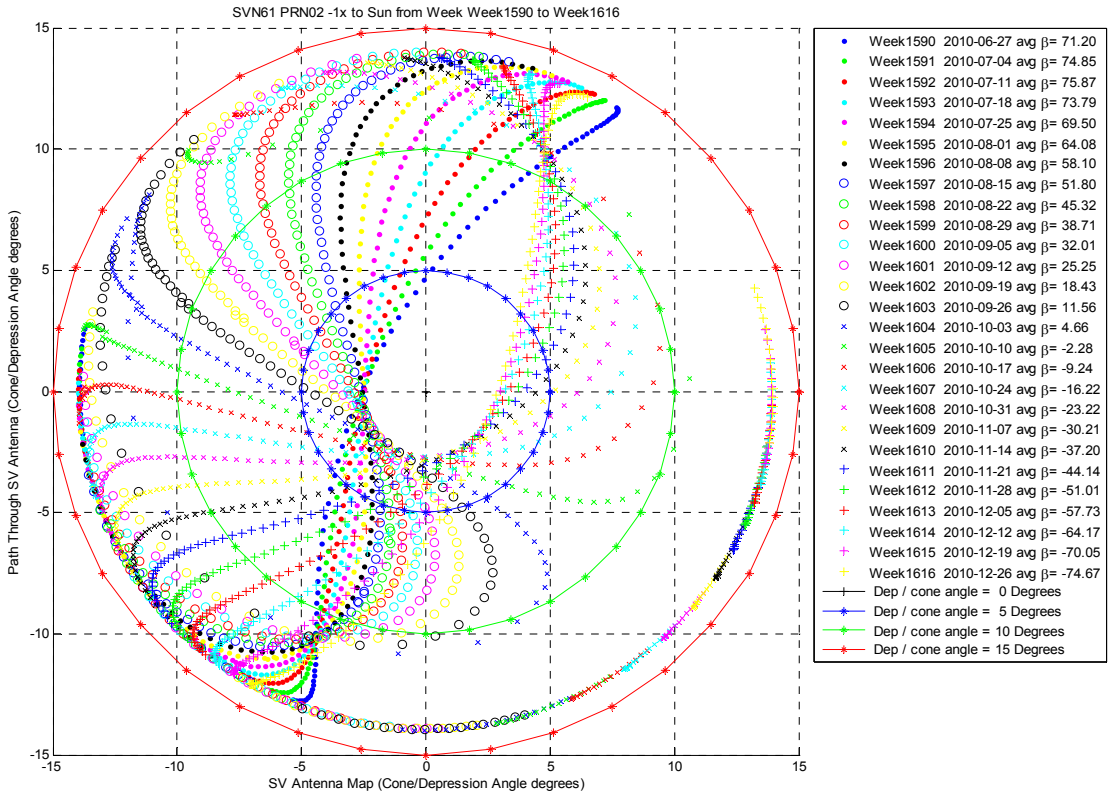

FIGURE A2: SAMPLE SV PASSES OVER 6 MONTHS (IIF SVN61)

The center point of the polar plot map is the θ = 0-degree nadir angle/boresight of the SV antenna, similar to the user polar plot sky maps with the center point of the polar plot being 90˚ elevation. The center point of the plot represents a SV directly overhead. If the SV does not pass directly overhead, then the SV polar plot will never cross through the θ equal to 0˚ boresight point just as an elevation path plot won't reach 90˚. Azimuth North becomes Azimuth relative to the satellite's x-axis. Data can only be acquired from SVs that happen to pass over the ground measurement site. This means that obtaining full visibility of a SV pattern from a ground site may take many years. That is why having intra-band data that is constant is important, it eliminates the need to see the full rise / set pass. Because one should check the azimuth symmetry assumption, one should either have multiple sites, or plan on monitoring the SV over a period sufficiently long to cover the SV antenna pattern as shown in figure A2.

In order to simplify the presentation of the path through the SV, a simplified xy plot using negative θ for rise, and positive θ for set is used. In some cases, the average of the rise and set values are taken for each θ to get a plot that only shows positive θ. When a plus and minus θ boresight angles are used, this is called an unwrapped boresight angle plot. When only positive θ is shown, this is called a wrapped boresight angle plot.

Appendix B: Quantitative Definition of Group Delay

Reference 1.1 defines group delay as the phase slope of the system transfer function. However, when the phase slope is not constant, the generalized maximum likelihood estimator for delay measurements needs to be used to account for bandwidth related effects. For this article, all of the relevant group delay/bandwidth effects are correctly handled by measuring the delays of the binary-phase-shift-keyed (BPSK) L1CA, L1P, L2C, and L5I/Q spreading signals using a P-chip early-minus-late tracking-loop, as specified by IS-GPS-200G 30.3.3.3.1 and IS-GPS-705. Specifically, IS-GPS-200G 30.3.3.3.1 states that all broadcast constants will be measured using a set of

specified tap spacings. Receiver vendors will be responsible for converting these broadcast values into values that are appropriate for their tracking loop implementation. For binary offset carrier signals (BOC), as well as for a more detailed mathematical treatment, ref 3.3 should be consulted.

Appendix C: Properties of the Ionosphere Free pseudorange equation

The generalization of the original ionosphere free pseudorange equation (3) for any code pair Lix,Ljz is

$$\rho_{Lix,Ljz} = \frac{\rho_{m_{Ljz}} - \gamma_{ij}\rho_{m_{Lix}}}{1-\gamma_{ij}} \quad \text{(10 or C1)}$$

This equation is designed to eliminate $1/f^2$ ionosphere errors and retain common mode terms such as the desired line of sight pseudorange ρ_{LOS}. However, any non-$1/f^2$, as well as noise are amplified. The details for how equation (C1/10) works is discussed below:

Insert the pseudorange measurement model equation (9) into equation (C1). Because equation (C1) is linear, we can analyze each term in equation (9), i.e., the individual code delay errors of $c\tau_{Lix}(\theta)$, the line of sight pseudorange, ρ_{LOS}, and the ionosphere term of $\frac{40.3TEC}{f_{Li}^2}$ individually. Any term in equation (9) that is identical to both pseudoranges (e.g. common terms) will remain in the final equation. Thus, the LOS term that is identical in each L-band pseudorange measurement pass through equation (C1) and contribute directly to the final iono free pseudorange:

LOS Term: $$\frac{(\rho_{LOS}) - \gamma_{ij}(\rho_{LOS})}{1-\gamma_{ij}} = (\rho_{LOS})\frac{1-\gamma_{ij}}{1-\gamma_{ij}} = (\rho_{LOS}) \quad \text{(C2)}$$

Any terms that varies with inverse frequency square cancel, thus the output of equation (C1) will be free of any ionosphere terms.

$$\rho_{Lix,Ljz} = 40.3\left[\frac{\frac{40.3TEC}{f_{Lj}^2} - \gamma_{ij}\frac{40.3TEC}{f_{Li}^2}}{1-\gamma_{ij}}\right] = 40.3\left[\frac{\frac{40.3TEC}{f_{Lj}^2} - \frac{f_{Li}^2}{f_{Lj}^2}\frac{40.3TEC}{f_{Li}^2}}{1-\frac{f_{Li}^2}{f_{Lj}^2}}\right] = 0 \quad 1/f^2 \text{ terms cancel (C3)}$$

Other terms come up as linear combinations, so if you insert the full measurement model Equation (9) into Equation (C1), you get the following.

$$\begin{aligned}\rho_{Lix,Ljz} &= \frac{\rho_{m_{Ljz}} - \gamma_{ij}\rho_{m_{Lix}}}{1-\gamma_{ij}} = \frac{[c\tau_{Ljz}(\theta) + \rho_{LOS} + n_{Lj,z}] - \gamma_{ij}[c\tau_{Lix}(\theta) + \rho_{LOS} + n_{Li,x}]}{1-\gamma_{ij}} \\ &= c\frac{\tau_{Ljz}(\theta) - \gamma_{ij}\tau_{Lix}(\theta)}{1-\gamma_{ij}} + \rho_{LOS} + \frac{n_{Ljz} - \gamma_{ij}n_{Lix}}{1-\gamma_{ij}}\end{aligned} \quad \text{(C4)}$$

Equation (C4) shows that although the ionosphere terms are eliminated, the delay errors of each signal being blended together leaves a bias error term of:

$$c\frac{\tau_{Ljz}(\theta) - \gamma_{ij}\tau_{Lix}(\theta)}{1-\gamma_{ij}} \quad \text{(10)}$$

To get a sense of the amplification factors in equation (C4) on any one individual term, if you insert the numerical frequency values for L1, L2, and L5 (L1=154*10.23 MHz = 1575.46 MHz, L2=120*10.23 MHz = 1227.6 MHz, and L5=115*10.23 MHz = 1176.45 MHz), then for L1 and L2:

$$\begin{aligned}\rho_{iono\_free\_L1L2} &= 2.5457\rho_{m_{L1PY}} - 1.5457\rho_{m_{L2PY}} \\ &= \rho_{LOS}(t) + 2.5457\,n_{fL1}(t) - 1.5457\,n_{fL2}(t)\end{aligned} \quad \text{(C5)}$$

For L1 and L5, the numerical weights are:

$$\begin{aligned}\rho_{iono\_free\_L1L5} &= 2.2606\rho_{m_{L1CA}} - 1.2606\rho_{m_{L5I/Q}} \\ &= \rho_{LOS}(t) + 2.2606\,n_{fL1}(t) - 1.2606\,n_{fL5}(t)\end{aligned} \quad \text{(C6)}$$

Using equation (C5), the RSS of the noise term amplifies the pseudorange error by $\sqrt{(\frac{1}{1-\gamma_{12}})^2 + (\frac{\gamma_{12}}{1-\gamma_{12}})^2}$. For L1 & L2 this is approximately 2.97 for identical strength independent random errors. The amplification factor for the L1 & L5 equation (C6) is approximately 2.58.

Appendix D: Alignment Equation Derivations

Aligning new dual L1&L2 frequency pairs to Dual L1PY&L2PY

Aligning any L1&L2 pair to dual L1PY&L2PY requires matching the difference between the two ionosphere free pseudoranges by adding an alignment term to the new pair to make its delay center equivalent to the reference $IFDC_{L1PYL2PY}$.

Dual Frequency Alignment Term for L1&L2:

$$DFAT_{L1x,L2z} = IFDC_{L1PY\&L2PY} - IFDC_{L1x,L2z} \quad \text{(D1)}$$

$$= c\frac{\tau_{L2PY}(\theta) - \gamma_{12}\tau_{L1PY}(\theta)}{1-\gamma_{12}} - c\frac{\tau_{L2z}(\theta) - \gamma_{12}\tau_{L1x}(\theta)}{1-\gamma_{12}} \quad \text{(D1a)}$$

$$= c\frac{[\tau_{L2PY}(\theta) - \tau_{L2z}(\theta)] - \gamma_{12}[\tau_{L1PY}(\theta) - \tau_{L1x}(\theta)]}{1-\gamma_{12}} \quad \text{(D1b)}$$

$$= c\frac{[IBD_{L2z}] - \gamma_{12}[IBD_{L1x}]}{1-\gamma_{12}} \quad \text{(D1c)}$$

Equation (D1c) shows that the L2 and L1 IBDs are sufficient to carry out any dual L1&L2 alignment with dual L1PY&L2PY. Since these IBD terms are more constant then the ISCs, they can be readily measured from any location that can see even a small portion of the SV antenna pattern.

Aligning new dual L1&L5 measurements to Dual L1PY&L2PY

Aligning any L1&L5 pair to dual L1PY&L2PY requires matching the difference between the two ionosphere free pseudoranges by adding an alignment term to the new pair to make it equivalent to the reference pair.

$$DFAT_{L1x,L5z} = IFDC_{L1PY\&L2PY} - IFDC_{L1x,L5z} \quad \text{z=L5I or L5Q} \quad \text{(D2)}$$

$$= c\frac{\tau_{L2PY}(\theta) - \gamma_{12}\tau_{L1PY}(\theta)}{1-\gamma_{12}} - c\frac{\tau_{L5z}(\theta) - \gamma_{15}\tau_{L1x}(\theta)}{1-\gamma_{15}} \quad \text{(D2a)}$$

$$= c\frac{\frac{1-\gamma_{15}}{1-\gamma_{12}}[\tau_{L2PY}(\theta)-\gamma_{12}\tau_{L1PY}(\theta)]-[\tau_{L5z}(\theta)-\gamma_{15}\tau_{L1x}(\theta)]}{1-\gamma_{15}} \quad \text{(D2b)}$$

If we add and subtract τ_{L1PY} to the first bracketed term, we can regroup equation (D2b) into a new form that only involves inter-band delays without the γ_{ij} scaling terms appearing in the differences. Pairs of inter-band delays can be measured as we will soon see. Appendix F carriers out all of the steps in re-arrangement of equation (D2c) back into IBD form (D2f).

$$DFAF_{L1xL5z} = c\frac{\frac{1-\gamma_{15}}{1-\gamma_{12}}[\tau_{L2PY}(\theta)-\gamma_{12}\tau_{L1PY}(\theta)+\tau_{L1PY}(\theta)-\tau_{L1PY}(\theta)]-[\tau_{L5z}(\theta)-\gamma_{15}\tau_{L1x}(\theta)]}{1-\gamma_{15}} \quad \text{(D2c)}$$

$$DFAF_{L1xL5z} = c\frac{\{[\tau_{L1PY}(\theta)-\tau_{L5z}(\theta)]-\frac{1-\gamma_{15}}{1-\gamma_{12}}[\tau_{L1PY}(\theta)-\tau_{L2PY}(\theta)]\}-\gamma_{15}[\tau_{L1PY}(\theta)-\tau_{L1x}(\theta)]}{1-\gamma_{15}} \quad \text{(D2d)}$$

$$DFAF_{L1xL5z} = c\frac{\{[ISC_{L5z}(\theta)]-(1-\gamma_{15})[T_{GD}]\}-\gamma_{15}[ISC_{L1x}(\theta)]}{1-\gamma_{15}} \quad \text{(D2e)}$$

As previously derived:

$$IBD_{L1x} = ISC_{L1x} \qquad (8a)$$
$$IBD_{L5z} = ISC_{L5z} - (1-\gamma_{15})T_{GD} \qquad (8c)$$

Thus equation (D2e) can be written in IBD form:

$$DFAF_{L1xL5z} = c\frac{\{[IBD_{L5z}(\theta)]\}-\gamma_{15}[IBD_{L1x}(\theta)]}{1-\gamma_{15}} \quad \text{(D2f)}$$

Aligning Single Frequency measurements to Dual L1PY&L2PY

Because the PPS and SPS users must both be supported, the single frequency alignment equations need to be developed. The delay center of any single frequency measurement on the i[th] Li band signal x is $c\tau_{Lix}(\theta)$. To align this profile with the $IFDC_{L1PY\&L2PY}$ profile, the Single Frequency Alignment Term ($SFAT_{Lix}$) needed is:

$$SFAT_{Lix} = c\tau_{Lix}(\theta) - c\frac{\tau_{L2PY}(\theta)-\gamma_{12}\tau_{L1PY}(\theta)}{1-\gamma_{12}} \quad \text{(D3a)}$$

As shown in Reference 3.1, the $IFDC_{L1PYL2PY}$ minus any single delay can be expressed as:

$$c\frac{\tau_{L2PY}(\theta)-\gamma_{12}\tau_{L1PY}(\theta)}{1-\gamma_{12}} - c\tau_{Lix}(\theta) = c(ISC_{Lix} - T_{GD}) \qquad \text{i=1,2,5} \quad \text{(D3b)}$$

Equation (D3b) appears in IS-GPS-200 but it is flipped in sign and expressed in seconds instead of being scaled into meters by the speed of light. In IS-GPS-200 section 20.3.3.3.2, the $SFAT_{L1PY}$ for L1PY pseudorange code alignment to dual L1PY&L2PY is given below, remembering that because ISC_{L1PY} = 0 by definition:

$$SFAT_{L1PY} = c\tau_{L1PY}(\theta) - c\frac{\tau_{L2PY}(\theta) - \gamma_{12}\tau_{L1PY}(\theta)}{1-\gamma_{12}} = -c(ISC_{L1PY} - T_{GD}) = cT_{GD}$$

(D4a)

The SFAT for L2PY pseudorange code alignment to dual L1PY&L2PY is given in the same section, noting the definition of T_{GD} as $ISC_{L2PY}/(1-\gamma)$, with $\gamma=\gamma_{12}$ if not otherwise specified:

$$SFAT_{L2PY} = c\tau_{L2PY}(\theta) - c\frac{\tau_{L2PY}(\theta) - \gamma_{12}\tau_{L1PY}(\theta)}{1-\gamma_{12}} = -c(ISC_{L2PY} - T_{GD}) = c[T_{GD} - (1-\gamma_{12})T_{GD}] = c\gamma_{12}T_{GD} \quad \text{(D4b)}$$

Finally in section 30.3.3.3.1.1.1, the hint of the general equation appears using L1CA code as a place holder for any other code on any carrier:

$$SFAT_{L1CA} = c\tau_{L1CA}(\theta) - c\frac{\tau_{L2PY}(\theta) - \gamma_{12}\tau_{L1PY}(\theta)}{1-\gamma_{12}} = c(T_{GD} - ISC_{L1CA}) \quad \text{(D4c)}$$

Equations (D3b and D4c) are important for several reasons: First it can be used to derive all the forms of the modernized and original ionosphere free equation. Second, it summarizes the mathematical linkage between the average value the Kalman filter uses for the $IFDC_{L1PYL2PY}$ and the JPL supplied T_{GD} value that must be maintained. Both of these topics are discussed next.

Using the Single Frequency Alignment term to derive the modernized Dual frequency algorithms

The SFAT, equation (D4c), can be used to derive the modernized dual frequency correction 30.3.3.3.1.1.2. If equation (1), repeated below, is used to form an ionosphere free pseudorange, any delays on the signals will appear in the output as an error.

$$\rho_{Lix,Ljz} = \frac{[\rho_{m_{Ljz}} - \gamma_{ij}\rho_{m_{Lix}}]}{1-\gamma_{ij}} \quad (1)$$

Pre-correcting each pseudorange by subtracting the $SFAT_{Lix}$ from each pseudorange will eliminate these errors. Inserting the SFAT factors for the Ljz and Lix pseudoranges into equation (1) results in:

$$\rho_{Lix,Ljz} = \frac{[\rho_{m_{Ljz}} - c(T_{GD} - ISC_{Ljz})] - \gamma_{ij}(\rho_{m_{Lix}} - c(T_{GD} - ISC_{Lix})]}{1-\gamma_{ij}} \quad \text{(D5) Pre-Corrected Form}$$

Factoring T_{GD} out of the numerator, equation (D5) is shown to be equivalent to equation (3) that was defined in section 30.3.3.3.1.1.2 of IS-GPS-200:

$$\rho_{Lix,Ljz} = \frac{[\rho_{m_{Ljz}} - \gamma_{ij}\rho_{m_{Lix}} + c(ISC_{Ljz} - \gamma_{ij}ISC_{Lix})]}{1-\gamma_{ij}} - cT_{GD} \quad \text{(3) Original Form}$$

As we presented in the overview section, a 3rd factoring of equation (3) can be done by moving T_{GD} into the 1st ISC term in (3) and identifying IBDs (using equations 8a-c) that are easier to measure is repeated below:

$$\rho_{L1x,Ljz} = \frac{[\rho_{m_{Ljz}} - \gamma_{1j}\rho_{m_{L1x}} + c(IBD_{Ljz} - \gamma_{1j}[IBD_{L1x}])]}{1-\gamma_{1j}} \quad \text{(7) IBD Form}$$

Thus we demonstrate that our IBD formulation of the ionosphere free pseudorange equation is equivalent to the original formulation and both result from the need to pre-correct the individual pseudoranges for SV equipment delays that are unique to each signal.

Using the Correct T_{GD} Value

We have shown that IBDs can accurately measure SV delay differentials. However, to be consistent with IS-GPS-200, we want to continue to broadcast ISCs, but there is one important caveat. Since the ISCs and T_{GD} are separately broadcast values, it is critical that their relationship is correctly maintained. When measured IBDs are converted via T_{GD} into the broadcast ISCs, they must utilize the currently broadcast T_{GD}. Otherwise a new error, related to the difference in T_{GD} value will result.

In addition, it is important to note that the CNAV ISC and T_{GD} values are quantized to a precision of 2^{-35} seconds (~0.03 nsecs) while the T_{GD} in subframe 1 is quantized by 2^{-31} or 0.465 nsecs. Thus, for modernized civil users, the CNAV T_{GD} is the more accurate value and should be used in preference to the legacy value.

Appendix E: IBD Measurement Algorithms

In this section, the measurements needed to fill in the IBD values are discussed. In addition, a strawman error budget is presented summarizing the accuracy of the measured IBDs being provided for the current CNAV messages and the resulting URE errors.

L1/L2 IBD measurements using Intra-Band Pseudorange Differences

In order to arrive at a means for measuring the IBDs, we will now show how to re-derive them in terms of GPS observable pseudoranges. The pseudorange measurement model equation (9) is repeated below:

$$\rho_{m_{Lix}} = c\tau_{Lix}(\theta) + \rho_{LOS} + \frac{40.3TEC}{f_{Li}^2} + n_{Lix} \quad (9),$$

The L1 and L2 IBDs are $IBD_{L1x} = [(\tau_{L1PY} - \tau_{L1x})]$ and $IBD_{L2z} = [(\tau_{L2PY} - \tau_{L2z})]$ respectively. This suggests forming intra-band pseudorange differences between signal x and signal z pseudoranges within the same i[th] band. The intra-band pseudorange yields:

$$\begin{aligned}\rho_{m_{Lix}} - \rho_{m_{Liz}} &= [c\tau_{Lix}(\theta) + \rho_{LOS} + \frac{40.3TEC}{f_{Li}^2} + n_{Lix}] - [c\tau_{Liz}(\theta) + \rho_{LOS} + \frac{40.3TEC}{f_{Li}^2} + n_{Liz}] \\ &= c[\tau_{Lix}(\theta) - \tau_{Liz}(\theta)] + \rho_{LOS} - \rho_{LOS} + 40.3[\frac{TEC}{f_{Li}^2} - \frac{TEC}{f_{Li}^2}] + [n_{Lix} - n_{Liz}] \quad \text{(E1a)} \\ &= c[\tau_{Lix}(\theta) - \tau_{Liz}(\theta)] + [n_{Lix} - n_{Liz}]\end{aligned}$$

The expected value, E[] of equation (E1a)

$$E[\rho_{m_{Lix}} - \rho_{m_{Liz}}] = c[\tau_{Lix}(\theta) - \tau_{Liz}(\theta)] + E[n_{Lix} - n_{Liz}] \quad \text{(E1b)}$$

If the measurement errors are zero mean, the intra-band delays can be measured.

As the L1 and L2 IBDs are always referenced to the PY code on the i[th] L band,

$$IBD_{Liz} = [\tau_{LiPY} - \tau_{Liz}] = \frac{E\left[\rho_{m_{LiPY}} - \rho_{m_{Liz}}\right]}{c}; i = 1,2 \quad \text{(E1c)}$$

An error budget analysis, presented later, will bound the zero mean noise assumption.

L1/L5 IBD measurements using two Inter-Band Pseudorange Differences

The L5 IBDL5z, with z=L5I or L5Q, is of the form:

$$\mathrm{IBD}_{\mathrm{L5z}} = [(\tau_{L1PY} - \tau_{L5z}) - (1-\gamma_{15})T_{GD}] = c\cdot[\tau_{L1,PY}(\theta) - \tau_{L5z}(\theta)] - c\cdot\frac{(1-\gamma_{15})}{(1-\gamma_{12})}\cdot[\tau_{L1,PY}(\theta) - \tau_{L2,PY}(\theta)] \quad \text{(8c)}$$

This consists of two inter-band delays, both using L1PY as a reference. Thus a reasonable starting point is to form two inter-band pseudorange differences and reference them to L1PY.

$$\begin{aligned}
\rho_{m_{Lix}} - \rho_{m_{Ljz}} &= [c\cdot\tau_{Lix}(\theta) + \rho_{LOS} + \frac{40.3TEC}{f_{Li}^2} + n_{Lix}] - [c\cdot\tau_{Ljz}(\theta) + \rho_{LOS} + \frac{40.3TEC}{f_{Lj}^2} + n_{Ljz}] \\
&= c\cdot[\tau_{Lix}(\theta) - \tau_{Ljz}(\theta)] + \rho_{LOS} - \rho_{LOS} + \frac{40.3TEC}{f_{Li}^2} - \frac{40.3TEC}{f_{Lj}^2} + [n_{Lix} - n_{Ljz}] \\
&= c\cdot[\tau_{Lix}(\theta) - \tau_{Ljz}(\theta)] + [\frac{40.3TEC}{f_{Li}^2}(1 - \frac{f_{Li}^2}{f_{Lj}^2})] + [n_{Lix} - n_{Ljz}] \\
&= c\cdot[\tau_{Lix}(\theta) - \tau_{Ljz}(\theta)] + [\frac{40.3TEC}{f_{Li}^2}(1-\gamma_{ij})] + [n_{Lix} - n_{Ljz}]
\end{aligned} \quad \text{(E2)}$$

In equation (E2), it is useful to factor the difference between the i=1 and j[th] ionosphere contribution, $\frac{40.3TEC}{f_{Li}^2} - \frac{40.3TEC}{f_{Lj}^2}$, into a form based on 1-γ_{1j} and yields: $[\frac{40.3TEC}{f_{Li}^2}(1-\gamma_{ij})]$.

If equation (E2) is now applied to both L1/L5 (Term1) and L1/L2 (Term2) to yield:

Term1: $\rho_{m_{L1PY}} - \rho_{m_{L5z}} = c\cdot[\tau_{L1PY}(\theta) - \tau_{L5z}(\theta)] + \frac{40.3TEC}{f_{L1}^2}(1-\gamma_{15}) + [n_{L1PY} - n_{L5z}]$ (E3a)

Term2: $\rho_{m_{L1PY}} - \rho_{m_{L2PY}} = c\cdot[\tau_{L1PY}(\theta) - \tau_{L2PY}(\theta)] + \frac{40.3TEC}{f_{L1}^2}(1-\gamma_{12}) + [n_{L1PY} - n_{L2PY}]$ (E3b)

Now difference Term1 and Term2 times (1-γ_{15})/(1- γ_{12}). This will convert the Term2 ionosphere TEC L1-L2 differential into a Term1 ionosphere TEC L1-L5 differential.

$$\begin{aligned}
Term1 - \frac{(1-\gamma_{15})}{(1-\gamma_{12})}\cdot Term2 &= [\rho_{m_{L1PY}} - \rho_{m_{L5z}}] - \frac{(1-\gamma_{15})}{(1-\gamma_{12})}[\rho_{m_{L1PY}} - \rho_{m_{L2PY}}] \\
&= c\cdot[\tau_{L1PY}(\theta) - \tau_{L5z}(\theta)] - c\cdot\frac{(1-\gamma_{15})}{(1-\gamma_{12})}\cdot[\tau_{L1PY}(\theta) - \tau_{L2PY}(\theta)] + \\
&\quad [n_{L1PY} - n_{L5z}] - \frac{(1-\gamma_{15})}{(1-\gamma_{12})}[n_{L1PY} - n_{L2PY}]
\end{aligned} \quad \text{(E4a)}$$

$$\begin{aligned}
E\{Term1 - \frac{(1-\gamma_{15})}{(1-\gamma_{12})}Term2\} &= E\{[\rho_{m_{L1PY}} - \rho_{m_{L5I}}] - \frac{(1-\gamma_{15})}{(1-\gamma_{12})}[\rho_{m_{L1PY}} - \rho_{m_{L2PY}}]\} \\
&= c\cdot[\tau_{L1PY}(\theta) - \tau_{L5z}(\theta)] - c\cdot\frac{(1-\gamma_{15})}{(1-\gamma_{12})}\cdot[\tau_{L1PY}(\theta) - \tau_{L2PY}(\theta)] + \\
&\quad \mathrm{E}\{[n_{L1PY} - n_{L5z}] - \frac{(1-\gamma_{15})}{(1-\gamma_{12})}[n_{L1PY} - n_{L2PY}]\} \quad \text{assuming zero mean noise} \\
&= c\cdot[\tau_{L1PY}(\theta) - \tau_{L5z}(\theta)] - c\cdot\frac{(1-\gamma_{15})}{(1-\gamma_{12})}\cdot[\tau_{L1PY}(\theta) - \tau_{L2PY}(\theta)] = IBD_{L5z}
\end{aligned} \quad \text{(E4b)}$$

As the IBD_{L5z} with z = L5I or L5Q is defined in equation (8c) as:

$$IBD_{L5z} = [(\tau_{L1PY} - \tau_{L5z}) - (1-\gamma_{15})T_{GD}] = c[\tau_{L1PY}(\theta) - \tau_{L5z}(\theta)] - c\frac{(1-\gamma_{15})}{(1-\gamma_{12})}[\tau_{L1PY}(\theta) - \tau_{L2PY}(\theta)] \quad (8c)$$

then, with proper calibrations so that the noise terms have zero mean, IBD_{L5z} can be measured using:

$$IBD_{L5z} = E\{[\rho_{m_{L1PY}} - \rho_{m_{L5z}}] - \frac{(1-\gamma_{15})}{(1-\gamma_{12})}[\rho_{m_{L1PY}} - \rho_{m_{L2PY}}]\} \quad (14c)$$

Because the L5 IBD required a $(1-\gamma_{15})/(1-\gamma_{12})$ scaling on the L1PY-L2PY inter-band delay, it was possible to cancel out the ionosphere term in the L1PY and L5z inter-band delays with the scaled L1PY-L2PY ionosphere term. Both Term1 and Term2 can be accurately measured as long as the dish antenna biases for L1PY, L2PY, and L5I/Q can be removed ensuring that all the noises are zero mean. Although the ionosphere contributions are cancelled out, because the L5 IBD relies on two inter-band measurements, the drawback is that there can be variations with boresight angle. If the entire SV antenna is not visible, an assessment for how well a constant approximates the entire L5 alignment term can't be made. This increases the uncertainty in the measurement.

Preliminary Error Budget

Table E1 shows a preliminary IBD Error Budget for the L1 and L2 IBDs, based on the methodologies in references 9.1-9.2. For each term, the source, assumed distribution, conversion or coverage factor used to arrive at the standard deviation, and the assumption used to arrive at a 95% confidence is discussed.

Term #	Term Description	Factors	Distribution notes	Coverage factor for distribution	Distribution Parameter	Other Factors	1σ error	2σ errors	units
1)	Jitter Error	1 Hz output	Gaussian	1.00	0.12	100 sec Smoothing	0.01	0.02	nsecs
		65 dBHz C/No				0.13 degree boresight resolution			
2)	Receiver Antenna Calibratoin within same band						0.00	0.00	nsecs
3)	Receiver Cal Errors for different codes on the same L band		Gaussian 3sigma 99%	6.00	0.20		0.03	0.07	nsecs
4)	CNAV/MNAV quanitzation		Uniform spec 1/2 width	1.73	0.01		0.01	0.02	nsecs
5)	Residual SV anisotrocipy	trending many patterns	Gaussian 3sigma 99%	6.00	0.30		0.05	0.10	nsec
6)	L1 or L2 IBD uncertainty						RSS	0.12	nsec
D1)	IBD2 uncertainty in a DFAT equation				IBD2 scaled by 1/(1-γ12)	-1.55		0.19	
D2)	IBD1 uncertainty in a DFAT equation				IBD1 scaled by γ12/(1-γ12)	-2.55		0.31	
N1)	Using 2 IBDs to form a DFAT		both IBDs have independent noises on them			(IBDL2-γIBDL1)/(1-γ) has a factor of ~3 amplification for equal and independent IBE1 and IBD2 noises	RSS	0.37	nsecs
N2)	SV Anistrocipy for the L1PYL2PY IFDC							use the JPL delay center profiles and a geometry URE simulation	

Table E1: L1 and L2 IBDs

The first term is the effect of thermal noise. A 10' parabolic dish antenna has a 30 dB gain and 5 degree beam width. The 30 dB dish plus minimum 35 dB-Hz terrestrial carrier to noise density ratio (C/No) yields 65 dB-Hz operation. With 1-second tracking loop output, P chip spacing, a front-end bandwidth of 30.69 MHz, 1 sigma uncertainty due to measurement noise is on the order of 0.12 nsec for the P code or civil codes with P chip spacing, (see Appendix B). Because IBDs are reasonably constants across the beam to within 0.3 nsec peak to peak variations (Figure 8), time averaging over the SV aperture to reduce the noise jitter is possible. To reduce jitter 10-

fold to 0.01 nsec, 10^2 or 100 seconds of 1-second tracking loop data filtering is needed. With 100 second zero delay shift filtering, over a typical 3 hour rise time covering 13.9 degrees boresight angle, the smoothed boresight resolution is reduced by the ratio of the filtering time to rise-time, or to 13.9*100/(3600*3) or 0.13 degrees, which is still giving reasonable resolution for assessing variations across the main beam.

Because a dish antenna is used, and is always pointing at the SV, there are no intra-band errors introduced by the dish antenna, so the 2nd term is zeroed out.

The 3rd term is receiver calibration so that each signal within each L-band has the same tracking error. The receiver calibration process is capable of +/- 0.1 nsec code alignments, or peak to peak errors of 0.2 nsec. Using a 3 sigma 99% Gaussian assumption, this gives a coverage factor of 6 to convert the peak to peak parameter into a 1 sigma statistic. Then the 95% 2 sigma scaling yields the 0.07 nsec error contribution.

The 4th term is the quantization of the ISC and IBD information. This is modelled as a uniformly distributed error of 0.029 nsec when using the 2^{-35} scaling factor in the CNAV messages. With a sqrt(12) coverage for the full LSB or sqrt(3) for the ½ sided value, and scaling back to 95% yields 0.02 nsec of error.

The 5th term is the residual intra-band anisotropy term due to small azimuth variations and beam edge effects. Based on trending of many of the satellites, a 0.3 nsec peak to peak 99% error is a reasonable first cut, and with coverage factor of 6 to convert peak to peak into a 1 sigma number, and then scaling by 2 to get 95% coverage yields a 0.1 nsec error.

The 6th term is the total 95% RSS (root sum square) error of all 5 terms is 0.12 nsec for each IBD. The final two sigma uncertainty of the L1 and L2 IBDs is 0.12 nsec.

To compute navigation errors, the DFAT alignment error (navigation error N1 in the table 1) and then the variation in the $IFDC_{L1PYL2PY}$ reference, navigation error line N2 in the table 1) has to be computed and then both terms RSS'd. Because it takes two IBDs scaled by the ionosphere free pseudorange equation to calculate the L1/L2 DFAT value, equation (D1c), lines D1 and D2 in table 1 calculate the multipliers. The RSS of the two DFAT factors results in a DFAT uncertainty of 0.37 nsecs (line N1). Note that this total could also be approximated by using the fact that the L1/L2 Ionosphere free pseudorange amplifies independent identical uncertainties by a factor of 3, or 3*0.12 nsec in line 6 yields a close approximation of 0.36 nsec in line N1.

The error due the L1PY&L2PY IFDC constancy assumption must be accounted for to arrive at a total URE. Using the JPL profiles in a Monte Carlo simulation is the best way to handle these terms (see appendices H-I). The alignment uncertainty (N1) and the $IFDC_{L1PYL2PY}$ uncertainty (N2) can then be RSS'd to get the final URE contribution to due to SV antenna anisotropy.

If the above analysis is repeated for the L5 IBDs, the following is error budget is obtained.

Term #	Term Description	Factors	Distribution notes	Coverage factor	Distribution Parameter	Other Factors	1σ error	2σ errors	units
1)	Jitter Error	1 Hz output	Gaussian	1.00	0.14	100 sec Smoothing	0.01	0.03	nsecs
		65 dBHz C/No				0.13 degree boresight resolution			
					p-p 99%				
2)	Receiver Antenna Cal Errors across different bands	guess	Gaussian 3sigma 99%	6.00	0.80	guess	0.13	0.27	
3)	CNAV/MNAV quanitzation		Uniform spec 1/2 width	1.73	0.01		0.01	0.02	nsecs
4)	Receiver Cal Errors		Gaussian 3sigma 99%	6.00	0.20		0.03	0.07	
					p-p 99%				
5a)	Residual SV anisotrocipy term1	trending many patterns	Gaussian 3sigma 99%	6.00	1.00	guess	0.17	0.33	nsec
5b)	Residual SV anisotrocipy term2	trending many patterns	Gaussian 3sigma 99%	6.00	1.00	guess	0.17	0.33	nsec
6)	L5 IBDL5 uncertainty						RSS	0.55	nsec
D1)	IBD5 multipler in DFAT equatoin				IBD5 scaled by $1/(1-\gamma 15)$	-1.26		0.69	
D2)	IBD1 multipler in DFAT equatoin				IBD1 scaled by $\gamma 15/(1-\gamma 15)$	-2.26		0.28	
N1)	Using 2 IBDs for a DFAT alignment						RSS	0.74	nsec
N2)	SV Anistrocipy for the L1PYL2PY IFDC							use the JPL delay center profiles and a geometry URE simulation	

Table E2: L5 preliminary IBD error budget (inter-band)

The first error, jitter noise, follows the same analysis of the IBD L1 and L2s except the noise is doubled in value because two measurements are used.

The second term in the L5 error budget requires estimates of the dish antenna calibration errors to be made. CNVA/MNAV quantization and Receiver calibration errors are terms 3 and 4, and are the same as for the IBD L1/L2 budget. For term 5, which consists of two inter-band delays, the SV anisotropy factors, because of limited IIF visibility, are estimates at this time. The total L5 IBD error is then RSS'd to arrive at line 5, the total L5 IBD uncertainty.

When the IBD L5 and IBD L1 factors are used to calculate the L1L5 DFAT value, equation (7, 15a), because they have different values, the individual multipliers in the L1/L5 ionosphere free operator of $1/(1-\gamma_{15})$ and $\gamma_{15}/(1-\gamma_{15})$ have to be used. This is done in lines D1 and D2. The RSS of lines D1 and D2 yields the total L1/L5 DFAT uncertainty in line N1. Finally, via a Monte Carlo simulation, the JPL profile effects can be used to assess the effects of the $IFDC_{L1PYL2PY}$ variations for line N2. The alignment uncertainty (N1) and the $IFDC_{L1PYL2PY}$ uncertainty (N2) can then be RSS'd to get the final URE contribution to due to SV antenna anisotropy.

Appendix F: L1&L5 Alignment Details

The first part of this appendix carriers out the L1&L5 alignment in more detail. The dual frequency alignment term for L1&L5 is given by equations (F1a and F1b) below,

$$c\frac{\tau_{L2PY}(\theta)-\gamma_{12}\tau_{L1PY}(\theta)}{1-\gamma_{12}} = c\frac{\tau_{L5z}(\theta)-\gamma_{15}\tau_{L1x}(\theta)}{1-\gamma_{15}} + DFAT_{L1xL5z} \qquad \text{(F1a)}$$

$$DFAT_{L1xL5z} = c\frac{\tau_{L2PY}(\theta)-\gamma_{12}\tau_{L1PY}(\theta)}{1-\gamma_{12}} - c\frac{\tau_{L5z}(\theta)-\gamma_{15}\tau_{L1x}(\theta)}{1-\gamma_{15}}$$

$$= c\frac{\frac{1-\gamma_{15}}{1-\gamma_{12}}[\tau_{L2PY}(\theta)-\gamma_{12}\tau_{L1PY}(\theta)]-[\tau_{L5z}(\theta)-\gamma_{15}\tau_{L1x}(\theta)]}{1-\gamma_{15}} \quad \text{(F1b)}$$

If we add and subtract τ_{L1PY} to the first bracketed term, terms in equation (F1b) can be regrouped into a new form that only involves inter-band delays without the γ_{ij} scaling appearing in the differences. Pairs of inter-band delays can be measured as we will soon see. We carry out the re-arrangement of equation (F1b) into two inter-band differences and one intra-band difference.

$$DFAT_{L1xL5z} = c\frac{\frac{1-\gamma_{15}}{1-\gamma_{12}}[\tau_{L2PY}(\theta)-\gamma_{12}\tau_{L1PY}(\theta)+\tau_{L1PY}(\theta)-\tau_{L1PY}(\theta)]-[\tau_{L5z}(\theta)-\gamma_{15}\tau_{L1x}(\theta)]}{1-\gamma_{15}} \quad \text{(F2)}$$

$$DFAT_{L1xL5z} = c\frac{\frac{1-\gamma_{15}}{1-\gamma_{12}}[\tau_{L2PY}(\theta)-\tau_{L1PY}(\theta)+\tau_{L1PY}(\theta)(1-\gamma_{12})]-[\tau_{L5z}(\theta)-\gamma_{15}\tau_{L1x}(\theta)]}{1-\gamma_{15}} \quad \text{(F3)}$$

$$DFAT_{L1xL5z} = c\frac{\frac{1-\gamma_{15}}{1-\gamma_{12}}[\tau_{L2PY}(\theta)-\tau_{L1PY}(\theta)]+[\tau_{L1PY}(\theta)(1-\gamma_{15})]-[\tau_{L5z}(\theta)-\gamma_{15}\tau_{L1x}(\theta)]}{1-\gamma_{15}} \quad \text{(F4)}$$

$$DFAT_{L1xL5z} = c\frac{\frac{1-\gamma_{15}}{1-\gamma_{12}}[\tau_{L2PY}(\theta)-\tau_{L1PY}(\theta)]-[\tau_{L5z}(\theta)-\tau_{L1PY}(\theta)]+\gamma_{15}[\tau_{L1x}(\theta)-\tau_{L1PY}(\theta)]}{1-\gamma_{15}} \quad \text{(F5)}$$

$$DFAT_{L1xL5z} = c\frac{\{[\tau_{L1PY}(\theta)-\tau_{L5z}(\theta)]-\frac{1-\gamma_{15}}{1-\gamma_{12}}[\tau_{L1PY}(\theta)-\tau_{L2PY}(\theta)]\}-\gamma_{15}[\tau_{L1PY}(\theta)-\tau_{L1x}(\theta)]}{1-\gamma_{15}} \quad \text{(F6)}$$

$$DFAT_{L1xL5z} = c\frac{\{[ISC_{L5z}]-\frac{1-\gamma_{15}}{1-\gamma_{12}}[ISC_{L2PY}]\}-\gamma_{15}[IBD_{L1x}]}{1-\gamma_{15}} \quad \text{(F7)}$$

$$DFAT_{L1xL5z} = c\frac{\{[ISC_{L5z}]-(1-\gamma_{15})[T_{GD}]\}-\gamma_{15}[IBD_{L1x}]}{1-\gamma_{15}} \quad \text{(F8)}$$

$$DFAT_{L1xL5z} = c\frac{\{[IBD_{L5z}]\}-\gamma_{15}[IBD_{L1x}]}{1-\gamma_{15}} \quad \text{(F9)}$$

where $IBD_{L5z} = [ISC_{L5z}]-(1-\gamma_{15})[T_{GD}]$ (8c)

Another way to look at the L5 IBD of $\{[\tau_{L1PY}(\theta)-\tau_{L5z}(\theta)]-\frac{1-\gamma_{15}}{1-\gamma_{12}}[\tau_{L1PY}(\theta)-\tau_{L2PY}(\theta)]\}$ is to think about $(1-\gamma_{15})/(1-\gamma_{12})$ being close to unity. If that factor were unity, the L5 IBD would be all L5 measurements relative to the L2 PY delay. While the exact compensation needed to align L1&L5 with L1&L2 requires making equation (F8) constant, an approximate way to tune the antenna would be to make the L5 profile have the same response as the

L2 profile. To assess how well this work, we write the L5 as an L2 + delta in equation (D1) below and assess the effects.

Alignment Error =

$$\begin{cases} \dfrac{\tau_{L2PY}-\gamma_{12}\tau_{L1PY}}{1-\gamma_{12}} - \dfrac{\tau_{L5,I/Q}-\gamma_{15}\tau_{L1,CA}}{1-\gamma_{15}} \text{ let } \tau_{L5,I/Q}=\tau_{L2PY}(\Theta_{SV})+\Delta\tau_{L2}(\Theta_{SV}) \text{ and } \tau_{L1,CA}= \tau_{L1,PY}(\Theta_{SV})+\Delta\tau_{L1}(\Theta_{SV}) \\ = \dfrac{\tau_{L2PY}(\Theta_{SV})-\gamma_{12}\tau_{L1PY}(\Theta_{SV})}{1-\gamma_{12}} - \dfrac{\tau_{L2PY}(\Theta_{SV})+\Delta\tau_{L2}(\Theta_{SV})-\gamma_{15}(\tau_{L1,PY}(\Theta_{SV})+\Delta\tau_{L1}(\Theta_{SV}))}{1-\gamma_{15}} = \\ [\tau_{L2PY}(\Theta_{SV})-\tau_{L1,PY}(\Theta_{SV})]\dfrac{\gamma_{12}-\gamma_{15}}{(1-\gamma_{12})(1-\gamma_{15})} - \dfrac{\Delta\tau_{L2}(\Theta_{SV})-\gamma_{15}\Delta\tau_{L1}(\Theta_{SV})}{1-\gamma_{15}} \end{cases} \quad \text{(F10)}$$

With

a) $$\gamma_{ij}=\left(\frac{f_{Li}}{f_{Lj}}\right)^2$$

b) L1=154*10.23 MHz, L2=120*10.23 MHz, and L5=115*10.23 MHz

c) L2z represents L2C, L5z represents codes of L5I or L5Q, and L1x represent L1CA.

d) θ_{SV} is the aperture dependent variation of any given code delay across the aperture of the satellite. We allow for both depression angle and azimuth angle variations, although the significant error only depends on depression angle.

The alignment deviations are as follows:

a) For every nsec of variation with boresight angle in the L1PY-L2PY profile, the net effect on the L1&L5 alignment is only .26 nsec per nsec as $\dfrac{\gamma_{12}-\gamma_{15}}{(1-\gamma_{12})(1-\gamma_{15})}$ is roughly -0.26 in value.

b) When you look at the effects of L2 minus L5 deviations, the 1/(1-γ_{15}) factor amplifies by -1.26, so every nsec of variation in boresight angle of L5 from L2, it causes a -1.26 alignment error.

c) Although the L1CA L1PY deviations are amplified, because L1CA and L1PY are in the same band with P chip spacings, there should be little contribution from this term.

Although SV antenna designs have focused on power, there are also SV antenna delay anisotropy considerations that will be important in future performance specifications.

Appendix G: Definitions of Published IBD and ISC Measurements

Intra-Band Delays

A 10' parabolic dish antenna has a 30 dB gain and 5 degree bandwidth. With minimum ICD power specifications for L2PY of -136 dBm and 3 dB noise figure, there is a baseline 35 dB-Hz C/No. Typically there is at least 65 dB-Hz carrier to noise density ratio with a 10' dish. With 1 second tracking loop output, 1 sigma uncertainty due to measurement noise is on the order of 0.1 nsec. This is based on both the receivers design test report circa 2007 PVT report that used the exact bandwidths for the receiver test asset, as well as using the nominal code loop uncertainty equations in ref 1.2 taken to the limit of high C/No for chip spacings of D that exceed the ratio of chip rate R_c to front end BW_{fe}, of:

$$\sigma_{codejitter} = T_{chip}\sqrt{\frac{B}{2C/No}D(1+\frac{2}{TC/No(2-D)})} \quad D>\frac{\pi R_c}{BW_{fe}} \qquad \text{(G1)}$$

Tchip nsec	C/No dBHz	C/No	BW	D	sigma jitter DLL nsecs
97.75	65.00	3162277.66	1.00	1.00	0.04
977.52	65.00	3162277.66	1.00	0.10	0.12

At the 65 dB-Hz limits, for P chip spacing, this yields 0.12 nsec performance in the 1 Hz bandwidth regime of operation. If we want a 10 fold reduction down to 0.01 nsec jitter, we need 10^2 = 100 seconds of 1 second tracking loop data. Over a 3 hour rise time covering 13.9 degrees of the SV nadir angle only degrades our nadir angle resolution by 13.9*100/(3600*3) to 0.13 degrees.

Although we can reduce code jitter to 0.01 nsecs, because intra-band delays have some small variations, we need to include some uncertainty in our estimates of the intra-band delays due to limited visibility of satellites at any one given time. We have not seen more than 0.3 nsec peak to peak variations for L1&L2, and we could be conservative to say that 1 sigma variations are well under 0.1 nsec.

The L5 intra-band delay is given by equations (8c, 15b) as:

$$\mathrm{IBD}_{\mathrm{L5}z} = \mathrm{ISC}_{\mathrm{L5}z} - (1-\gamma_{15})\,\mathrm{T}_{\mathrm{GD}} = \{[\tau(\theta)_{L1PY} - \tau(\theta)_{L5z}] - \frac{(1-\gamma_{15})}{(1-\gamma_{12})}[\tau(\theta)_{L1PY} - \tau(\theta)_{L2PY}]\} \qquad \text{(8c)}$$

$$\mathrm{IBD}_{\mathrm{L5}z} = [\rho_{m_{L1PY}} - \rho_{m_{L5z}}] - \frac{(1-\gamma_{15})}{(1-\gamma_{12})}[\rho_{m_{L1PY}} - \rho_{m_{L2PY}}] = c\,[\tau_{L1PY}(\theta) - \tau_{L5z}(\theta)] - c\,\frac{(1-\gamma_{15})}{(1-\gamma_{12})}[\tau_{L1PY}(\theta) - \tau_{L2PY}(\theta)] + [n_{L1PY} - n_{L5z}] - \frac{(1-\gamma_{15})}{(1-\gamma_{12})}[n_{L1PY} - n_{L2PY}] \qquad \text{(15b)}$$

Performance is limited by SV visibility. Currently, many of the IIF satellites don't get enough coverage at our site to show how well the L2 and L5 patterns are matched. Over time, the IIF orbits will drift into view to allow the entire pattern to be mapped out.

The receiver asset being used is also calibrated across all codes. Because of the extreme accuracies being required, it was not possible to find a test transmitter that is better calibrated than the receiver. The calibration algorithm does specialized I/Q channel swapping so that both the test transmitter and receiver are calibrated at the same time. The calibration has been shown to be independent of the test transmitter being used.

Once the intra-band differentials are measured, equations (8a-c) plus the broadcast T_{GD} value for each satellite is used to create constant ISC values from the IBDs for that satellite. These constant ISC values work for the dual frequency corrections because T_{GD} drops out for dual frequency alignments. In the previous sub-section, we

showed that as long as we add back in the same T_{GD} that the master Kalman filter has factored in, then equations (8a-c) create constant ISCs that make the same approximations built into the ephemeris based on dual L1PY&L2PY profiles being a constant.

Delta Code Delta Carrier, Ionosphere free code and carrier, and Wide-Lane Cross Checks

We are able to cross check our results and examine azimuth variations with several other measurements. We can directly compute the difference between any two ionosphere free pairs, as shown in figure 8 or figure 10. As one approaches the edge of the beam, the constant intra-band differential delay assumption breaks down and the measurements become less stable as the 5 degree beam gets near the ground at the 5 degree elevation angles.

In order to directly measure the profile variations of absolute delay errors $\tau(\theta)_{Lix}$ (figure 5), ISC_{Lix} values (figure 4), and ionosphere free pseudoranges $\rho_{Lix,Liz}$ of all different pairs (figure 6), combined code and carrier phase processing can be used as described in ref 3.2. Because the ionosphere delay has equal and opposite signs for the code and carrier measurements, it can be eliminated by adding together code and carrier measurements at the cost of introducing a carrier phase ambiguity. By differencing two different signal pairs, the common line of sight true (error free) pseudorange can be eliminated. Because delta pseudorange as measured by the carrier loop has a whole number of integer carrier cycles, all of the carrier measurements require an additional measurement to eliminate the unknown number of carrier phase cycles, as well as some other hardware induced errors. By using the broadcast T_{GD} value, the carrier cycle and hardware induced errors can be accounted for. But without seeing the entire beam, the T_{GD} calibration can be in error. The shape will be correct, but the vertical axis alignment will have arbitrary floating phase cycle. The key equations from reference 3.2 are given below in the form of measured pseudoranges and measured integrated carrier phase measurements, assuming the measurements are made with a steerable beam antenna that always points at the SV. The ranging measurement from the code loop (that is affected by the group velocity of the signal), and the carrier measurement (affected by the phase velocity of the signal) are given below, with terms we wish to isolate in red, ionosphere terms we wish to eliminate in purple, and true (error free) LOS range dynamics that we wish to eliminate in cyan.

Code based measurements:

$$\rho_{m_{L1,x}}(t) = \rho_{LOS}(t) + \frac{A(t)}{f_{L1}^2} + c \bullet \tau_{L1,x}(\Theta_{SV}(t)) + c \bullet \tau_{dish\_rcvr_{L1}} \quad \text{(G2a)}$$

$$\rho_{m_{L2,z}}(t) = \rho_{LOS}(t) + \frac{A(t)}{f_{L2}^2} + c \bullet \tau_{L2,z}(\Theta_{SV}(t)) + c \bullet \tau_{dish\_rcvr_{L2}} \quad \text{(G2b)}$$

Integrated Carrier based delta range measurements using an unknown number of carrier cycles to express the measurement in terms of a full ideal error free cyan colored line of sight pseudorange term:

$$\lambda_{L1}\theta_{m_{L1,x}}(t) = \rho_{LOS}(t) - \frac{A(t)}{f_{L1}^2} + \lambda_{L1} \bullet N_{L1} + \lambda_{L1} \bullet \underbrace{\theta_{SV_{L1}}(\Theta_{SV}(t))}_{\sim 0} + \lambda_{L1} \bullet \theta_{dish\_rcvr_{L1}} + \ldots \quad \text{(G3a)}$$

$$\lambda_{L2}\theta_{m_{L2,z}}(t) = \rho_{LOS}(t) - \frac{A(t)}{f_{L2}^2} + \lambda_{L2} \bullet N_{L2} + \lambda_{L2} \bullet \underbrace{\theta_{SV_{L2}}(\Theta_{SV}(t))}_{\sim 0} + \lambda_{L2} \bullet \theta_{dish\_rcvr_{L2}} + \ldots \quad \text{(G3b)}$$

By using a dish antenna that is always pointing at the satellite as it rises and sets, any contribution to the delay and phase of the received signal by the receiving dish antenna is a constant over the entire pass.

To measure the beam angle changes in the In the ISC values, metric #1 from reference 3.2, of delta code minus delta carrier measurements, is used to isolate the ISC values as shown below:

$$M1 = [\rho_{m_{L1,PY}}(t) - \rho_{m_{L2,z}}(t)] + [\lambda_{L1}\theta_{m_{L1,x}}(t) - \lambda_{L2}\theta_{m_{L2,z}}(t)] = c \bullet ISC_{L2,z}(\Theta_{SV}(t)) + c \bullet [\tau_{dish\_rcvr_{L1}} - \tau_{dish\_rcvr_{L2}}] + \lambda_{L1} \bullet N_{L1} - \lambda_{L2} \bullet N_{L2} + (\lambda_{L1} \bullet \theta_{dish\_rcvr_{L1}} - \lambda_{L2} \bullet \theta_{dish\_rcvr_{L2}}) \quad \text{(G4)}$$

T_{GD} can be used to perform the calibration to eliminate the other terms, assuming we see the same amount of the beam that the monitor station and JPL did when calculating T_{GD}. Because we can't guarantee that assumption, measuring the intra-band differential delays, and then calibrating by T_{GD} is now the standard procedure we use to publish ISC values.

To measure the beam angle changes in the different ionosphere free pseudorange pairs (metric #2 in reference 3.2), we can form the code based ionosphere free pseudorange and the carrier based ionosphere free pseudorange to difference out the common range terms.

$$M2_{generalized} = \{\frac{\rho_{m_{Lj,z}} - \gamma_{1j} \bullet \rho_{m_{L1,x}}}{1-\gamma_{1j}}\} - \{\frac{\lambda_{Lj}\theta_{m_{Lj,z}} - \gamma_{1j} \bullet \lambda_{L1}\theta_{m_{L1,x}}}{1-\gamma_{1j}}\} = c \bullet \frac{\tau_{Lj,z}(\Theta_{SV}(t)) - \gamma \bullet \tau_{L1,x}(\Theta_{SV}(t))}{1-\gamma} + \ldots$$
$$c \bullet \frac{\tau_{dish\_rcvr_{Lj}} - \gamma_{1j} \bullet \tau_{dish\_rcvr_{L1}}}{1-\gamma_{1j}} - \frac{N_j\lambda_{Lj} - \gamma N_1 \bullet \lambda_{L1}}{1-\gamma_{1j}} - \frac{\lambda_{Lj}\theta_{dish\_rcvr_{Lj}} - \gamma_{1j}\lambda_{L1}\theta_{dish\_rcvr_{L1}}}{1-\gamma_{1j}} \quad \text{(G5)}$$

In order to observe the angular variations of the individual i[th] L-band x[th] signal's delay error, wide lane metrics can be used. For example, when looking at the L1PY beam angle variations, metric #3 below can be used:

$$M3_{L1PY} = [\rho_{m_{L1,PY}}(t) - \lambda_{L1}\theta_{m_{L1,PY}}(t)] + 2[\frac{\lambda_{L2}\theta_{m_{L2,PY}}(t) - \lambda_{L1}\theta_{m_{L1,PY}}(t)}{\gamma - 1}] \quad \text{(G6)}$$
$$= c \bullet \tau_{L1,PY}(\Theta_{SV}(t)) + c \bullet \tau_{dish\_rcvr_{L1}} - \lambda_{L1} \bullet N_{L1} - \lambda_{L1} \bullet \theta_{dish\_rcvr_{L1}} - 2\{\frac{\lambda_{L2} \bullet N_{L2} - \lambda_{L1} \bullet N_{L1} + \lambda_{L2} \bullet \theta_{dish\_rcvr_{L2}} - \lambda_{L1} \bullet \theta_{dish\_rcvr_{L1}}}{(1-\gamma)}\}$$

Other individual code's delay error profiles can also be formed

Appendix H: 24 Hour Line of Sight Analysis of errors due to Constant $IFDC_Y$ profile assumptions

To get a sense of the size of the current errors relative to a proposed modernized performance standard, consider the projections of what the Modernized Precise Positioning Performance Standard might look like, shown below in Figure H1 taken from reference 2.3, circa the year 2000.

Table 4. New UERE Budget for the Modernized GPS

UERE Component Allocations and Sums, meters rms

Allocation	Dual-Frequency P(Y)-Code Receivers			Dual-Frequency C/A-Code Receivers			Single-Frequency P(Y)-Code Receivers			Single-Frequency C/A-Code Receivers		
Space Segment												
Clock Stability	0.5			0.5			0.5			0.5		
Group Delay Stability	0.3			1.1			0.5			1.6		
Diff'l Group Delay Stability	1.0			3.3			0.0			0.0		
Selective Availability (SA)	N/A			0.0			N/A			0.0		
Other Satellite Errors	0.3			0.3			0.3			0.3		
Space Subtotal	1.2			3.5			0.8			1.7		
Control Segment	Terrestrial		Space	Terrestrial		Space	Terrestrial		Space	Terrestrial		Space
Clock/Ephemeris Estimation	0.8		0.9	0.8		0.9	0.8		0.9	0.8		0.9
Clock/Ephemeris Prediction	0.5		0.9	0.5		0.9	0.5		0.9	0.5		0.9
Clock/Ephemeris Curve Fit	0.4		0.4	0.4		0.4	0.4		0.4	0.4		0.4
Other Clock/Ephemeris	0.3		0.3	0.3		0.3	0.3		0.3	0.3		0.3
Iono Delay Model Terms	N/A		N/A	N/A		N/A	4.9-9.8		4.9-9.8	7.4-14.7		7.4-14.7
Group Delay Time Estimate	N/A		N/A	N/A		N/A	2.3		2.3	2.3		2.3
Control Subtotal	1.1		1.4	1.1		1.4	5.5-10.1		5.6-10.2	5.5-10.1		5.6-10.2
Subtotal, Space & Control	*1.6*		*1.8*	3.7		3.8	5.6-10.1		5.7-10.2	5.8-10.3		5.8-10.3
Reduction by WAGE*	*1.0*			N/A			1.0			N/A		
Total Signal-in-Space (SIS)	1.3		1.5	3.7		3.8	5.5-10.1		5.6-10.2	5.8-10.3		5.8-10.3
User Segment**	Air	Surface	Space	Air	Surface	Space	Air	Surface	Space	Air	Surface	Space
Receiver Noise	0.2	0.2	0.4	0.2	0.2	0.4	0.2	0.2	0.4	0.2	0.2	0.4
Multipath	0.1	0.9	0.0	0.1	0.9	0.0	0.1	0.9	0.0	0.1	0.9	0.0
Ionospheric Delay	0.4	1.4	0.6	0.4	1.4	0.6	0.0	0.0	0.0	0.0	0.0	0.0
Tropospheric Delay	0.5	0.5	0.0	0.5	0.5	0.0	0.5	0.5	0.0	0.5	0.5	0.0
Other UE Errors	0.4	0.4	0.4	0.4	0.4	0.4	0.4	0.4	0.4	0.4	0.4	0.4
User Subtotal	0.8	1.8	0.8	0.8	1.8	0.8	0.7	1.1	0.6	0.7	1.1	0.6
Total System UERE	1.5	2.2	1.7	3.8	4.1	3.9	5.5-10.1	5.6-10.2	5.6-10.2	5.8-10.3	5.9-10.3	5.9-10.3

* Or other means of minimizing the effective age of data (AOD) to ≤ 3 hr

** All-in-view receiver; State 5 navigation using carrier-based deltaranges with P(Y)-code, or State 8 navigation using carrier smoothed code with C/A-code

556

FIGURE H1: PROJECTED UERE COMPONENT ALLOCATIONS FOR THE MODERNIZED GPS SATELLITES, METERS RMS

If one considers that the PY code Ionosphere free delay variations are part of the "Other Satellite Errors which eventually could be split into antenna anisotropy and Other errors", these terms would have to be less than the 95% 2 sigma number of 2 x 0.3 = 0.6 meter. (The official Feb 2007 performance standard uses 2 sigma 95% numbers, while reference 2.3 uses 1 sigma rms specifications and is shown in figure H2. Comparing Figure H1 with Figure H2, the current PPS performance standard, other satellite error term 2 sigma number is 1 meter or 1 sigma, 0.5 meter.

Table A.4-1. Dual-Frequency P(Y)-Code UERE Budget Without WAGE

Segment	Error Source	UERE Contribution (95%) w/o WAGE (meters)		
		Zero AOD	Max. AOD in Normal Operation	14.5 Day AOD
Space	Clock Stability	0.0	8.9	257
	Group Delay Stability	0.0	0.6	0.6
	Diff'l Group Delay Stability	0.0	2.0	2.0
	Satellite Acceleration Uncertainty	0.0	2.0	204
	Other Space Segment Errors	1.0	1.0	1.0
Control	Clock/Ephemeris Estimation	2.0	2.0	2.0
	Clock/Ephemeris Prediction	0.0	6.7	206
	Clock/Ephemeris Curve Fit	0.8	0.8	1.2
	Iono Delay Model Terms	N/A	N/A	N/A
	Group Delay Time Correction	N/A	N/A	N/A
	Other Control Segment Errors	1.0	1.0	1.0
User*	Ionospheric Delay Compensation	4.5	4.5	4.5
	Tropospheric Delay Compensation	3.9	3.9	3.9
	Receiver Noise and Resolution	2.9	2.9	2.9
	Multipath	2.4	2.4	2.4
	Other User Segment Errors	1.0	1.0	1.0
95% System UERE (PPS)		7.5	13.8	388
* For illustration only, actual PPS receiver performance varies significantly -- see Table B.2-1				

FIGURE H2: CURRENT PPS ERROR BUDGET, 95% 2 SIGMA NUMBERS ARE IN THIS TABLE

By inserting the JPL errors from figure I1 into a typical satellite visibility program, one can form the elevation, SV depression angle, and $IFDC_Y$ errors as a function of depression angle, and then measure the statistics and histogram the distribution of the line of sight errors over 24 hours to compute the probability densities. Figure G3 shows the results for two sample satellites, SVN61 and SVN59; the computation can be repeated on a larger scale over a number of world-wide locations. The errors won't be Gaussian over 24 hours, rather more like a U-shaped distribution as shown in the bottom plots of Figure H3. In Figure H4, the distribution of average errors over all LOSs over a 24 hour period shows that the errors meet error budget projections, as long as the variations in Figure I1 don't significantly change with any A/B side switching or other configuration changes.

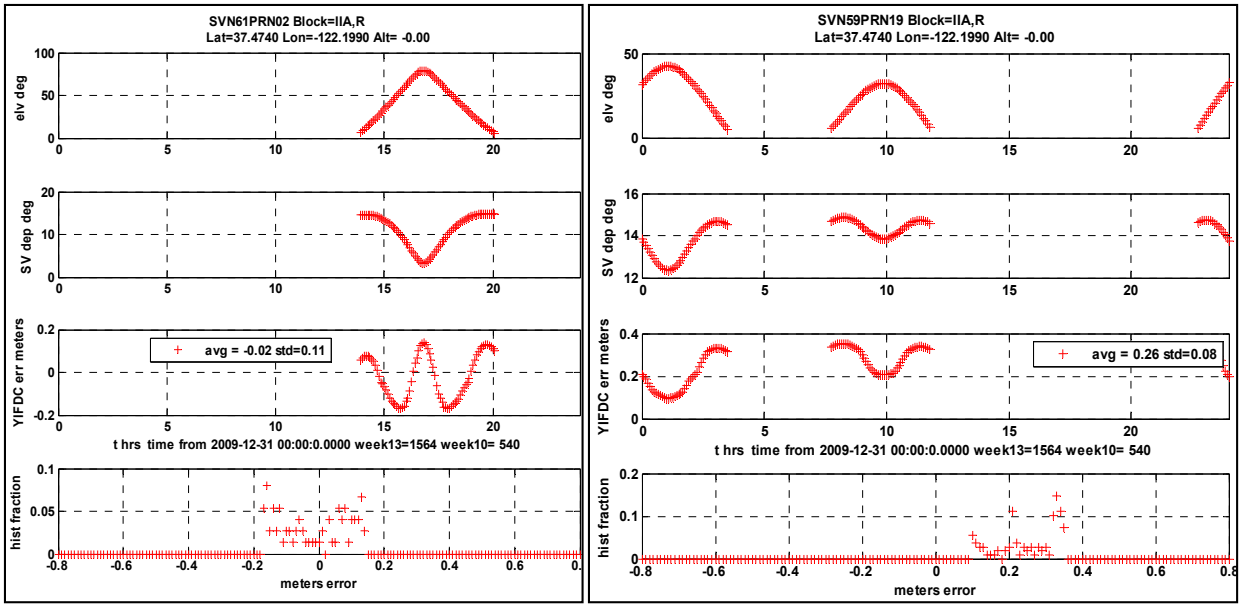

FIGURE H3: SIMULATION OF IFDCY VARIATIONS FOR DEC 31, 2009, CONSTELLATION ORBITS

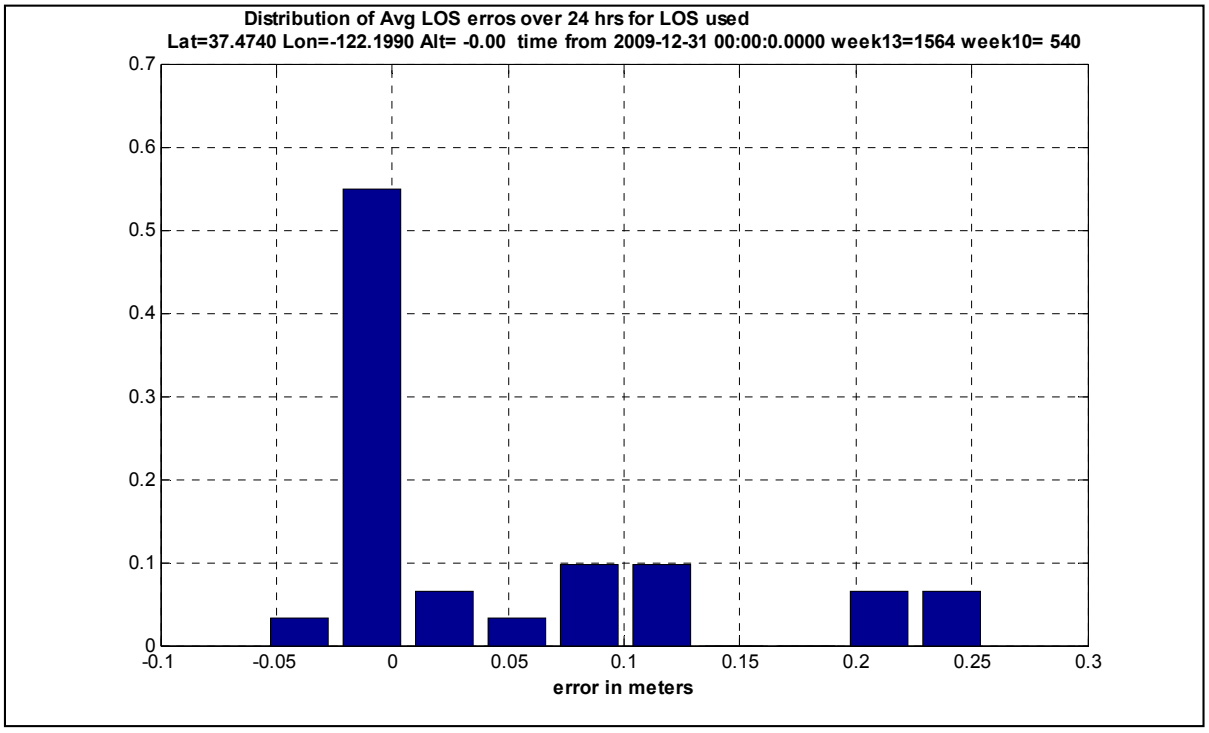

FIGURE H4: HISTOGRAM OF A DEC 2009 24 HOUR SNAP SHOT OF MEAN L1&L2 ERRORS DUE TO $IFDC_Y$ VARIATIONS

Appendix I: JPL's 2006 to 2009 Measurement of $IFDC_{L1PYL2PY}$ Delay and Phase Errors

Because the ionosphere free measurement Equation (3) represents a blend of the L1 signal that emanates from an L1 delay center and the L2 signal that emanates from an L2 delay signal, we define the Ionosphere Free Delay Center (IFDC) as a blend of the L1PY and L2PY delay centers. If the L1PY and L2PY delay center locations vary with boresight angle, the IFDC has its own unique boresight angle profile given by Equation (12). Equation (12) represents the SV antenna anisotropy variations with boresight angle.

$$\mathrm{IFDC}_{L1PY,L2PY} = \mathrm{c}\frac{\tau_{L2PY}(\theta) - \gamma_{12}\tau_{L1PY}(\theta)}{1-\gamma_{12}} \quad (12)$$

JPL used an orbiting semi-codeless P code receiver to directly measure the dual PY code IFDCs for all SV satellites in orbit during the 2006 to 2009 time period; see Reference 6.1. Figure I1 taken from Reference 6.1 shows JPL's results, with the IIR-M portion of the original figure enlarged to improve readability.

First, it is important to note that JPL measured both the phase center and delay center SV antenna anisotropy terms of the current SVs. Both are needed. The antenna delay center curves directly show the ephemeris error as a function of SV nadir/boresight angle θ when using code based pseudorange measurements, the officially supported measurement in IS-GPS-200 (figure 20-3). However, some high precision surveying receivers also perform PPP (Precise Point Positioning) which use carrier phase techniques and attempt to eliminate all of the carrier phase ambiguities. For a full pseudorange measurement using carrier phase, the location of the SV phase center becomes important. For this paper, we will focus on the delay center variations, although for historical reasons as pointed out earlier, phase center had been the term that was being used

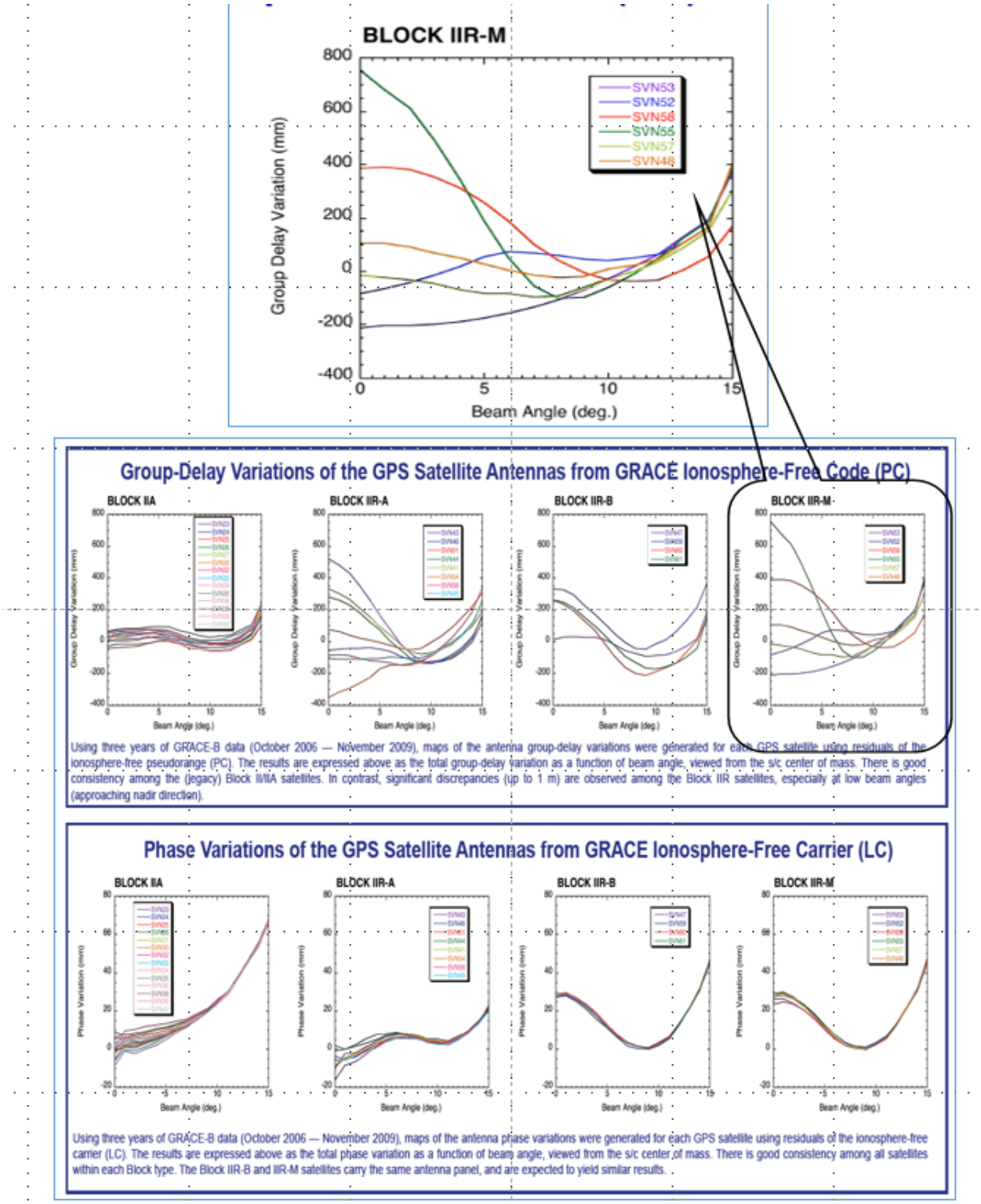

FIGURE I1 JPL DUAL Y CODE IONO-FREE DELAY CENTER VARIATIONS AS A FUNCTION OF SV NADIR ANGLE (REFERENCE 6.1)

Figure I1 shows that the IIR-M satellites have the largest delay center variations, ½ to ¾ meter variations across the beam. Although these variations are within the current Precise Positioning Performance Standards (ref 2.2), personal communication with engineers who contribute definitions to the ICDs indicate that a future modernized performance standard would include terms like these in an SV antenna anisotropy category.

Because of the differencing and weighting by the γ scaling factor in Equation (12), it is possible for the IFDC to be located behind the antenna deck. This might seem contrary to intuition, which is to expect the emanation point for the L1 or L2 signal along any one of the helical elements to be roughly at the midpoint of the helix. However, recall that the SV antenna is an array and as noted in Reference 1.2, array antennas can have distinct and different phase and delay centers than that of their elements.

For many of the GPS satellites, the precise ephemeris for the antenna phase center (APC, which we think should be called antenna delay center ADC) shows the signal is emanating from behind the SV helical mounting deck. Looking at late 2014 and early year 2015 precise ephemeris data, we can see evidence that for the IIR-M GPS satellites, the delay center is located behind the antenna deck. The NGA has two precise ephemeris products: center of gravity (CG), and antenna phase center (APC). Subtracting the NGA APC precise ephemeris data from the NGA CG precise ephemeris data demonstrates that the APC and CG locations for the IIR-M satellites are within 5 cm of each other. Since the IIR-M CG is behind the antenna deck, so too is its APC. In contrast, the APC and CG locations for the IIF satellites are distinct; the horizontal offset is 0.39 m, and the APC is about 1.09 m closer to the earth the than the CG. Reference 8, Choi, 2002, provides phase center measurements and dimensions for a prototype IIF satellite. In particular, there is a 0.39 meter lateral lever arm from the CG axis of the satellite to the center of the array, confirming the NGA IIF CG minus APC lateral offset. For the IIA satellites, the horizontal offset is 0.28 meters and the radial offset is 0.95 m closer to the Earth, about the same as for the IIF. Like the IIR-Ms, the IIR satellites have no horizontal offset, but the APC is about 1.5 meters closer to the Earth than the CG. Without additional measurements for the IIR, IIA, and IIF, the location of the APC can't be conclusively placed behind or in front of the antenna deck. The wide range of horizontal and radial offsets from the GPS SV types currently on orbit make it clear that intuition is no substitute for measurement when it comes to understanding the full behavior of the IFDC for all pairs of codes.